

TESTS OF QCD AT LOW x

H. ABRAMOWICZ

*School of Physics and Astronomy
Raymond and Beverly Sackler Faculty of Exact Sciences
Tel Aviv University, Israel*

This talk reviews the latest measurements of the proton, Pomeron and photon structure functions. These measurements, especially at low x and/or low Q^2 lead to new insight into the picture of hadronic interactions.

1 Introduction

One of the big challenges within Quantum Chromodynamics (QCD) as the theory of strong interactions is the understanding of its role in describing the approach to the non-perturbative, soft interactions, at least at a qualitative level if not quantitative.

The soft hadron-hadron interactions are well described by the Regge phenomenology in which the interaction is viewed as due to exchanges of Regge poles. The Regge poles can be classified into different families according to their quantum numbers. The Regge poles with quantum numbers of mesons form linear trajectories in the m^2, l plane, where m is the mass of the meson and l its spin. The continuation of a trajectory to negative values of m^2 leads to a parameterization in terms of t , the square of the four momentum transfer, as follows:

$$\alpha(t) = \alpha_0 + \alpha' \cdot t, \quad (1)$$

where α_0 is the intercept and α' is the slope of the trajectory. Among all possible families of Regge poles there is a special one, with the quantum numbers of the vacuum, called the Pomeron (\mathbb{P}) trajectory. There are no known bound states lying on this trajectory (glueballs would be expected to form this trajectory) and its parameters have been determined experimentally^{1,2,3,4}

$$\alpha_{\mathbb{P}} = 1.08 + 0.25t. \quad (2)$$

In Regge theory the energy dependence of total and elastic cross sections is derived from the analytic structure of the hadronic amplitudes. In the limit $s \gg -t$, where s is the square of the center of mass energy of the scattering, the amplitude for elastic scattering has the form $A(s, t) \sim s^{\alpha_{\mathbb{P}}(t)}$. The Pomeron trajectory also provides the leading

contribution to the high energy behavior of the total cross section,

$$\sigma_{\text{tot}} = s^{-1} \text{Im}A(s, t=0) \propto s^{\alpha_{\mathbb{P}}(0)-1} \quad (3)$$

The s dependence of hadronic interactions fulfills this behavior independently of the interacting particles^{4,5} as expected from the universality of the exchanged trajectories.

The deep inelastic charged lepton-proton interactions at low momentum transfers can be viewed as due to virtual photon proton interactions, γ^*p , with the flux of photons originating from the incoming lepton. The F_2 structure function of the proton is related to the total absorption cross section $\sigma_{\text{tot}}(\gamma^*p)$,

$$F_2(x, Q^2) \simeq \frac{Q^2(1-x)}{4\pi^2\alpha} \sigma_{\text{tot}}(\gamma^*p), \quad (4)$$

where x and Q^2 are the Bjorken scaling variable and the negative of the mass square of the virtual photon respectively. In deep inelastic scattering (DIS) the kinematical region which corresponds to the Regge limit is that of low x at fixed Q^2 due to the relation,

$$x = \frac{Q^2}{W^2 + Q^2 - m_p^2}, \quad (5)$$

where W denotes the center of mass energy of the γ^*p system and m_p the mass of the proton. For large Q^2 , DIS can be analyzed in the framework of perturbative QCD based on the factorization theorem, the ensuing QCD evolution equations and the quark-parton model description of the hadrons. The transition between the perturbative regime and the non-perturbative regime may provide an understanding of the soft interactions in the language of QCD and establish whether the Regge model can be justified from first principles.

The first step in this direction has been made with the measurements of the electromagnetic proton structure function F_2 which cover now a range in Q^2 from 10^{-1} to 10^4 GeV^2 and in x from 10^{-6} to about 1. The first evidence for soft like interactions at large Q^2 came with the appearance of events with a large rapidity gap in the hadronic final state in low x interactions at HERA.^{6,7} These events, when interpreted in terms of Pomeron exchange, allow a first glance at the partonic structure of this fundamental ingredient of the Regge approach. Last but not least the combined data from HERA and LEP start exploring the structure of the photon in the low x region.

2 The structure functions of the proton

2.1 F_2

The most precise measurements of the proton structure function with the widest coverage of the phase space come from electro and muon-production. At this conference new measurements of the F_2 proton structure function have been presented by the NMC,⁸ H1⁹ and ZEUS¹⁰ experiments. The existing coverage of the phase space in $1/x$ and Q^2 is summarized in figure 1. Also included are the previous measurements of the SLAC,¹¹ BCDMS^{12,13} and E665¹⁴ experiments.

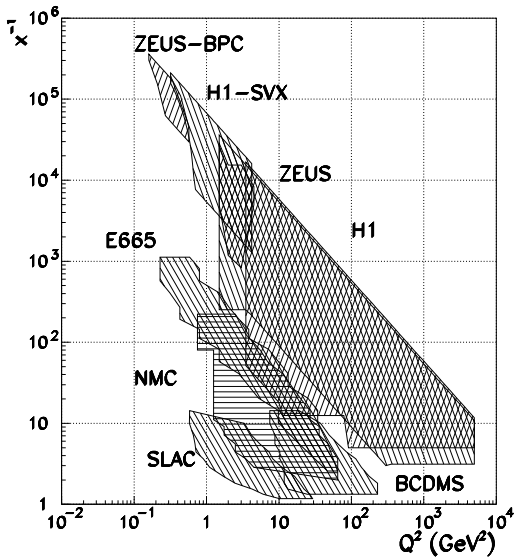


Figure 1: Phase space coverage of the F_2 measurements.

One of the striking properties of F_2 is that

it rises strongly with decreasing x , contrary to expectations based on the Regge approach and in line with the properties of the QCD evolution equations.^{15,16} This is shown in figure 2 where the recent ZEUS measurements¹⁰ are compared with some of the existing parameterizations of F_2 down to $Q^2 = 1.5$ GeV^2 .

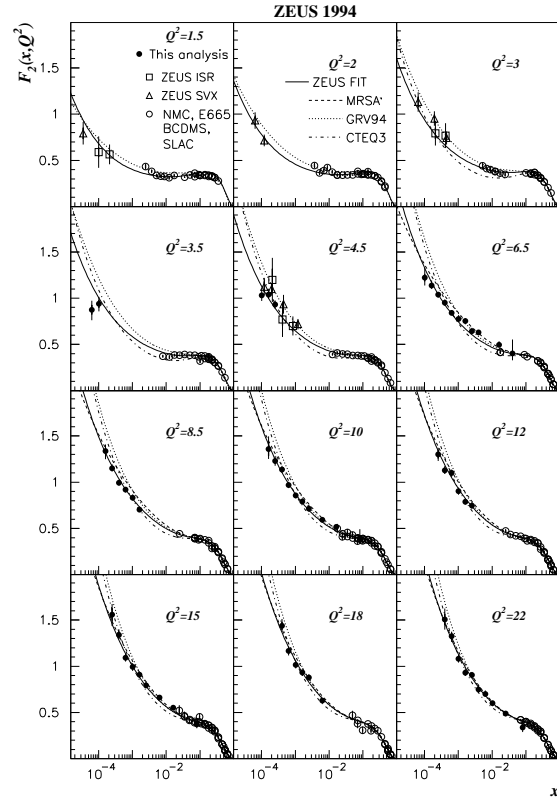


Figure 2:

An example of the x dependence of F_2 at low x as measured by the ZEUS experiment. Also shown are selected parameterizations of parton distributions as denoted on the figure^{17,18,19} and the NLO QCD fit performed by ZEUS.

Since, as has been measured at HERA,^{20,21} the total photoproduction cross section is known to increase only slowly with energy, the question which remained opened till this conference was to establish at which value of Q^2 the structure function stops rising with decreasing x . New data were presented by the ZEUS Collaboration²² based on measurements performed with the Beam Pipe Calorimeter which covers the range $0.16 < Q^2 < 0.65$ GeV^2 . The new measurements of H1²³

from a special run covering the range $0.35 < Q^2 < 3.5 \text{ GeV}^2$ close the remaining gap in Q^2 . As seen in figure 3, up to $Q^2 \sim 0.85 \text{ GeV}^2$ the data favor parameterizations which are based on the dominance of soft interactions in this region such as the one of Donnachie and Landshoff²⁴ or the CKMT²⁵ one in which, due to screening corrections, the effective intercept of the bare Pomeron is Q^2 dependent. For larger Q^2 values, $Q^2 \geq 1.2 \text{ GeV}^2$, the GRV¹⁸ and BK²⁶ parameterizations, perceived in this region as representative of the solution of the NLO DGLAP QCD evolution equations,^{27,28,29} give a very good description of the data.

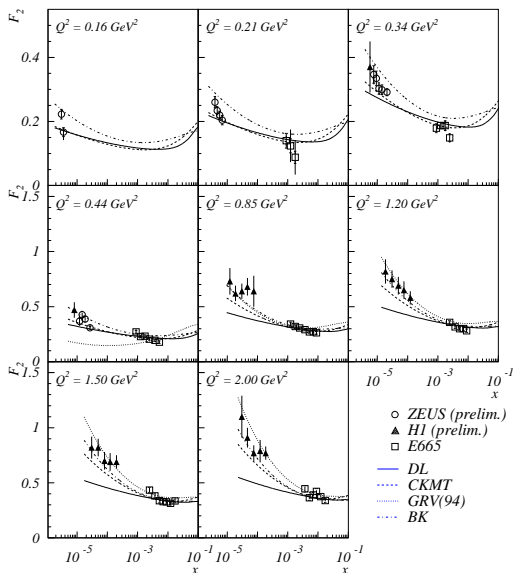


Figure 3:

Preliminary measurements of the proton structure function $F_2(x, Q^2)$ at low Q^2 by the H1 and ZEUS experiments together with results from the E665 experiment compared to model predictions as explained in the text.

The behavior of F_2 as a function of Q^2 for selected values of x is presented in figure 4. The structure function F_2 rises strongly with Q^2 for $x < 0.01$, over three decades in Q^2 in some regions of x where the data are available. With the new data the gap between the fixed target experiments and the HERA experiments has been filled and a good agreement in the overlap region is observed.

2.2 Structure functions and perturbative QCD

In perturbative QCD the electromagnetic structure function F_2 is represented as a convolution of the parton distributions and coefficient functions $C(x, Q^2)$ proportional to the effective γ^* -parton couplings,

$$\frac{1}{x} F_2(x, Q^2) = \sum_{i=1}^{n_f} e_i^2 C_i(x, Q^2) \otimes (q + \bar{q})(x, Q^2) + C_g(x, Q^2) \otimes g(x, Q^2), \quad (6)$$

where q denotes quarks of charge e_i and g gluons, \otimes stands for a convolution integral and n_f is the number of contributing flavors. The parton distributions evolve with Q^2 following the DGLAP equations,

$$\frac{\partial}{\partial \ln Q^2} \begin{pmatrix} q \\ g \end{pmatrix} = \frac{\alpha_s(Q^2)}{2\pi} \begin{bmatrix} P_{qq} & P_{qg} \\ P_{gq} & P_{gg} \end{bmatrix} \otimes \begin{pmatrix} q \\ g \end{pmatrix}, \quad (7)$$

where α_s denotes the strong coupling constant. Given a specific factorization and renormalization scheme, the coefficient functions C_i and splitting functions P_{ij} are obtained in QCD by perturbative expansion. In particular

$$P_{ij}(x, Q^2) = \frac{\alpha_s}{2\pi} P_{ij}^{(1)}(x) + \left(\frac{\alpha_s}{2\pi}\right)^2 P_{ij}^{(2)}(x) + \dots \quad (8)$$

The truncation after the first two terms in the expansion defines the conventional NLO DGLAP evolution. This evolution assumes that the dominant contribution to the DIS cross section comes from parton cascades in which partons from subsequent emissions are strongly ordered in transverse momenta k_t , the largest corresponding to the parton interacting with the probe.

At low x higher-loop contributions to the splitting functions are enhanced,

$$P_{ij}^{(n)} \sim \frac{1}{x} \ln^{(n-1)} x. \quad (9)$$

The presence of these terms may spoil the convergence of (8). The evolution equation which allows the resummation of leading $(\alpha_s \ln x)^n$ contributions and which describes parton radiation without k_t ordering is known under the name BFKL.^{30,31,32} In the parton cascade picture this contribution corresponds roughly to cascades which develop from a large $k_t \sim Q$ parton emitted at large x and the rest of the evolution takes

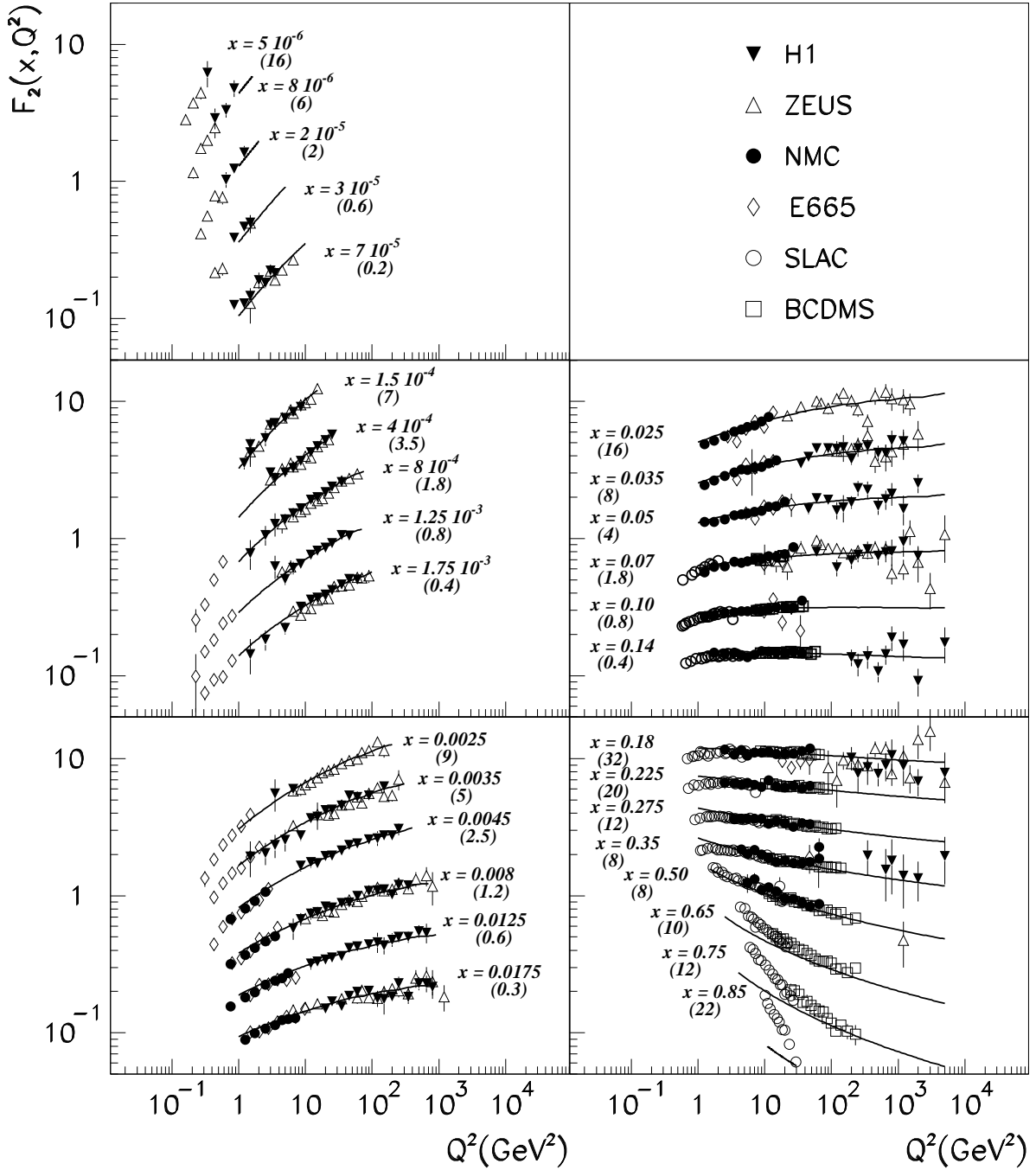


Figure 4: Compilation of measurements of F_2 as a function of Q^2 for selected values of x as denoted on the figure. The numbers in parenthesis are the scaling factors by which the value of F_2 has been multiplied in the plot. The overlaid curves are the result of an NLO QCD fit performed by the H1 experiment.

place only in x . The two approaches, the DGLAP and the BFKL one are embodied in the CCFM equation,^{33,34,35} based on the k_t factorization and angular ordering.

The solutions of the DGLAP equations and of the BFKL equation, in the limit of very low x , where the dominant contribution to the cross section is driven by gluon radiation, predict a rise of F_2 with decreasing x ,

$$F_2^{DLL}(x, Q^2) \sim \exp \left(2 \sqrt{\frac{C_A \alpha_s}{\pi} \ln \frac{1}{x} \ln \frac{Q^2}{Q_0^2}} \right), \quad (10)$$

$$F_2^{BFKL}(x, Q^2) \sim \sqrt{\frac{Q^2}{Q_0^2}} x^{-\frac{4C_A \alpha_s}{\pi} \ln 2} \quad (11)$$

where the superscript DLL stands for the double leading logarithmic approximation used in solving the DGLAP equation and Q_0^2 denotes the starting scale of the evolution. In general the BFKL equation predicts a faster increase of F_2 with decreasing x and stronger scaling violations in Q^2 as compared to the DGLAP evolution. However the solution (11) is derived assuming a constant α_s and higher order corrections are expected to tame the rise with $1/x$.³⁶ In the BFKL approach the concept of a QCD Pomeron arises naturally.

The confrontation of the various approaches with the data requires assumptions on the input parton distributions which cannot be derived from first principles. The solution of the NLO DGLAP evolution equations with input parton distributions fitted to the data has been widely explored^{18,19,37,38,39,40} and gives a very good description of the data, down to amazingly low values of Q^2 . An example is shown in figure 4 where the NLO parameterization of F_2 obtained by H1⁹ is presented. The data were fitted for $Q^2 > 7 \text{ GeV}^2$ and evolved backwards down to $Q^2 = 1 \text{ GeV}^2$.

A byproduct of the NLO DGLAP fits to the data is the NLO gluon distribution in the proton. If the value of α_s is known the gluon distribution at low x is constrained by the logarithmic slope of F_2 in Q^2 . The gluon distributions obtained at $Q^2 = 20 \text{ GeV}^2$ by the respective experimental groups, which can handle best the correlated systematic errors, are presented in figure 5. Also shown for comparison are the results obtained earlier with smaller statistics. The improvement is evident. One may be led to conclude that,

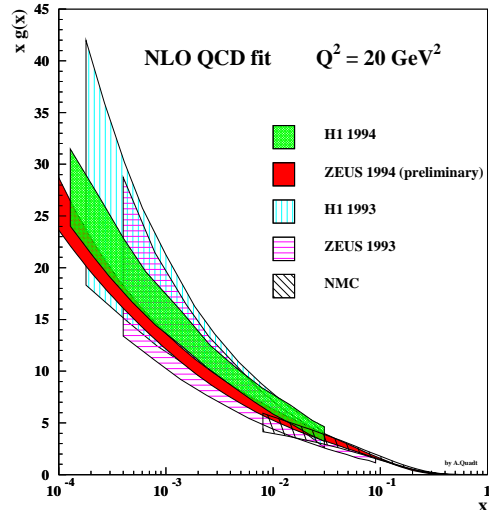


Figure 5:
Gluon distribution in the proton as determined from NLO QCD fits to the F_2 data.

since the data are perfectly described by the NLO DGLAP, there is no evidence for new QCD dynamics at low x . However one should keep in mind that a set of equations based only on F_2 measurements is under-constrained. This is because, while F_2 is directly proportional to the quark distributions (see equation (6)),

$$\frac{\partial F_2}{\partial \ln Q^2} \propto P_{gg} \otimes g, \quad (12)$$

and the gluon distribution is reliable only to the extent to which P_{gg} is known. Ways of constraining the system are to measure either the longitudinal structure function F_L and/or the charm contribution to F_2 .^{41,42,43}

2.3 F_L

The lack of knowledge of F_L limits the experimental accuracy with which F_2 can be determined. The relation between the measured electromagnetic differential DIS cross section and the F_2 and F_L structure functions is the following:

$$\frac{d^2\sigma}{dx dQ^2} = \frac{2\pi\alpha^2}{xQ^4} [(1 + (1 - y)^2) F_2 - y^2 F_L]. \quad (13)$$

At low x , that is high y , the contribution of F_L is non-negligible and cannot be ignored. The usual

procedure adopted experimentally is to use, in the region of moderate x , the parameterization of the ratio $R \approx F_L/(F_2 - F_L)$ based on the dedicated SLAC measurements⁴⁴ and, at low x , the QCD expectations based on existing parton distributions.

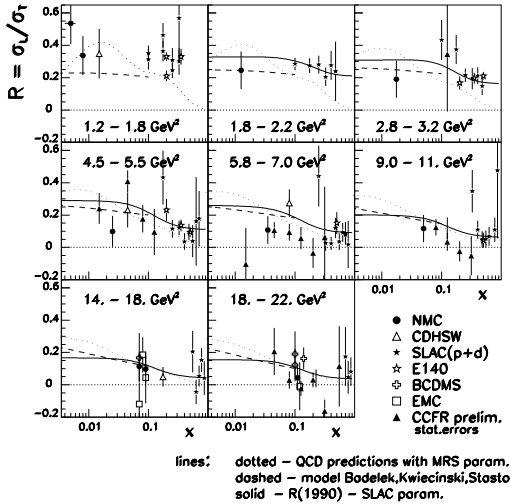


Figure 6:

Measurements of R as a function of x in bins of Q^2 , compared to the SLAC (full line), QCD NLO MRS(R1) (dotted line) and Badełek et al. (dashed line) parameterizations.

The experimental determination of $R = \sigma_L(\gamma^*p)/\sigma_T(\gamma^*p)$, where L, T stand for the longitudinal and transverse polarization of the virtual photon, requires the measurement of the differential cross section (13) at different center of mass energies and fixed x, Q^2 . New measurements of R have been presented at this conference by the NMC Collaboration⁸ which has used muon-production data taken at four different muon beam momenta ranging from 90 to 280 GeV. Preliminary results have been also presented by the CCFR Collaboration^{45,46} based on $(\bar{\nu})$ Fe in the neutrino energy range from 10 to 350 GeV. The new measurements extend the range of x down to $x \sim 10^{-3}$ at the lowest $Q^2 \sim 1.5$ GeV². The compilation of all existing data is presented in figure 6. The measurements are compared to three different parameterizations, the SLAC one,⁴⁴ the new parameterization of Badełek et al.⁴⁷ presented at this conference and to the QCD expectations based on the new MRS(R1) parameterization of

parton distributions.³⁸ As can be seen from this comparison all of them reproduce the data fairly well, although they may differ up to 50% at low x .

In order to constrain the value of F_L in the low x regime explored at HERA, the H1 Collaboration determined F_L assuming that the NLO DGLAP evolution holds.²³ The parameterization of F_2 was obtained using only the data for $y < 0.35$, where the contribution of F_L is small (see formula (13)). The difference between the value of F_2 expected from this parameterization at larger y and the one determined from the cross section assuming $F_L = 0$ is then used to determine the required F_L . The results of this procedure are shown in figure 7. Also shown are the expectations for F_L obtained from the same QCD fit and assuming that $F_L = F_2$. Within errors there is a consistency between the values obtained from the procedure above and the QCD fit, again pointing to the fact that the NLO QCD evolution is describing the data very well.

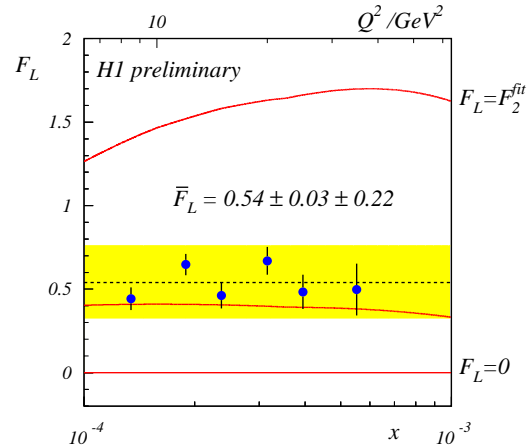


Figure 7:

F_L as a function of x (and Q^2) as determined by the H1 experiment. The full line closest to the data corresponds to NLO QCD expectations.

2.4 $F_2^{c\bar{c}}$

The measurement of charm production is of utmost importance. The perturbative QCD calculations involving heavy quarks are most reliable due to the large masses involved. It may turn out that charm production cross sections will provide the best constraint on the gluon distribution in the

proton.⁴⁸ Experimentally though, large integrated luminosities are needed because of the low tagging efficiency of charm in the final state.

The first glance at the charm production properties in DIS have been presented by the H1²³ and ZEUS⁴⁹ experiments, based on statistics of the order of 100 events or so. Experimentally charm production was tagged by reconstructing the D^0 (H1) or the D^* (H1 and ZEUS) mesons and their charge conjugates. The signal of $D^0 \rightarrow K\pi$ decay as seen in the H1 detector is presented in figure 8.

The D^* decays are identified by the decay chain

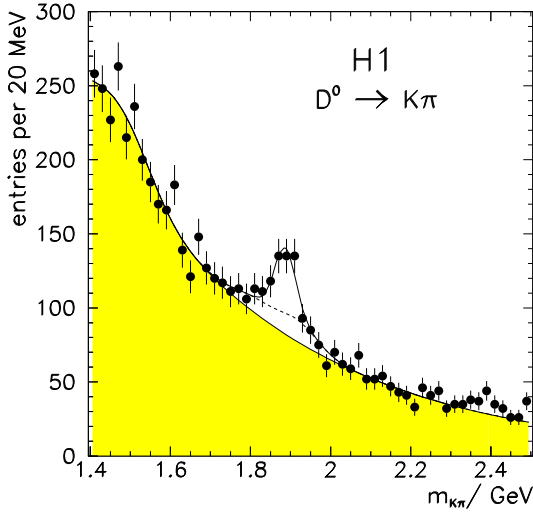


Figure 8:

The invariant mass spectrum of $K\pi$ as seen in the H1 detector.

$D^* \rightarrow D^0\pi \rightarrow K\pi\pi$, taking advantage of the tight kinematic constraint imposed by the small mass difference $\Delta M = m_{D^*} - m_{D^0} = 145.5 \pm 0.15$ MeV. As an example the signal observed in the ΔM distribution in the ZEUS analysis is shown in figure 9.

The dominant mechanism of charm production in DIS at HERA energies is the boson-gluon fusion process. Indeed the AROMA⁵⁰ MC based on the boson gluon fusion mechanism is found to reproduce properly the shapes of the transverse momentum and pseudorapidity of the D mesons as well as the overall W and Q^2 dependence. An upper limit of 5% for a possible contribution of the charm sea has been estimated by the H1 experiment.

The ZEUS experiment finds that also the absolute value of the measured cross section is well reproduced by the boson gluon fusion mechanism

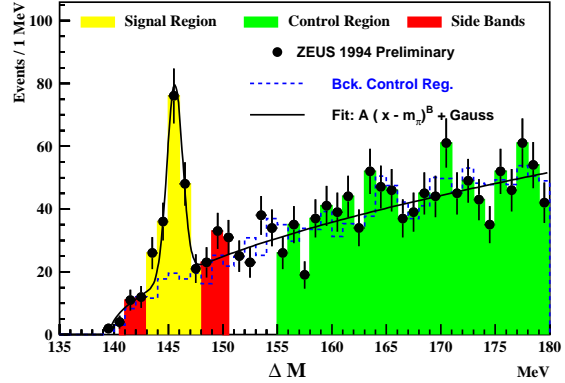


Figure 9:

The $\Delta M = m(K\pi\pi_s) - m(K\pi)$ distribution for $m(K\pi)$ in the D^0 signal region, where π_s denotes the softest pion.

calculated to LO, if the appropriate GRV gluon distribution¹⁸ is used in the simulation and if the mass of the charm quark is kept within the limits $1.35 \leq m_c \leq 1.5$ GeV.

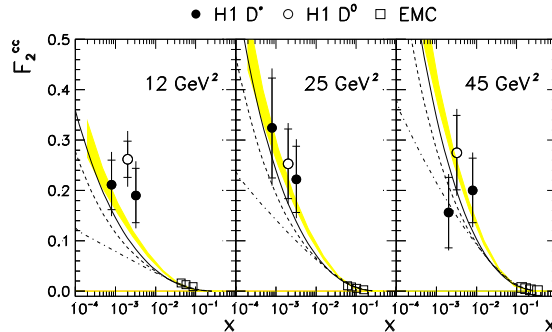


Figure 10:

F_2^{cc} as measured by the H1 experiment. The curves correspond to various QCD parton parameterizations. The shaded area is the expectation based on the H1 NLO QCD fit.

The charm production cross section measured by the H1 experiment is found to be larger than expected from NLO calculations for any known gluon distributions. This can partly be seen in figure 10 where the F_2^{cc} as determined by H1 is compared to NLO QCD expectations.

Comparison of the H1 results with the EMC⁵¹ data reveals a steep rise of F_2^{cc} from $x \sim 0.1$ to $10^{-3} < x < 10^{-2}$. Averaged over the measured

kinematic range of H1 a ratio $\langle F_2^{c\bar{c}}/F_2 \rangle = 0.237 \pm 0.021^{+0.043}_{-0.039}$ is obtained, one order of magnitude larger than at larger x .

2.5 α_s from DIS

An important ingredient of the perturbative QCD analysis of the F_2 structure function is the value of $\alpha_s(M_Z^2)$ assumed in the fits. The CCFR Collaboration has presented preliminary results from their study of $(\bar{\nu})$ Fe interactions.⁴⁵ The evolution of the $x F_3$ structure function allows a direct determination of α_s . The preliminary value presented at this conference is $\alpha_s(M_Z^2) = 0.118 \pm 0.007$ to be compared with 0.113 ± 0.005 previously determined from a combined fit to the SLAC/BCDMS F_2 evolution⁵² and 0.122 ± 0.004 from the global LEP fit to the electroweak data.⁵³ The good news is that now the value of α_s determined from the DIS and the LEP data are in good agreement.

2.6 Conclusions

The structure function of the proton F_2 is found to be rising with decreasing x down to Q^2 as low as 1 GeV². At moderate $Q^2 \sim 10$ GeV², the rise can be quantified by $F_2 \sim x^{-0.2 \div -0.3}$ and it becomes faster at higher Q^2 . The observed trend is very well described by the conventional DGLAP evolution in NLO. However this observation does not disprove the existence of new dynamics at low x . This is because the system is under-constrained and a combination of unknown parton distributions with different splitting functions can mimic the observed behavior of $F_2(x, Q^2)$. To test this point measurements of the longitudinal structure function F_L and/or the charm contribution to F_2 are essential. The existing measurements are far too imprecise. Some indications that the k_t ordering implied by the DGLAP evolution may not be the full story comes from studies of the hadronic final states.⁵⁴ Another reason to look beyond the standard evolution is that $F_2(x, Q^2)$ cannot rise indefinitely with decreasing x without violating the unitarity bound.

3 Diffractive Hard Scattering

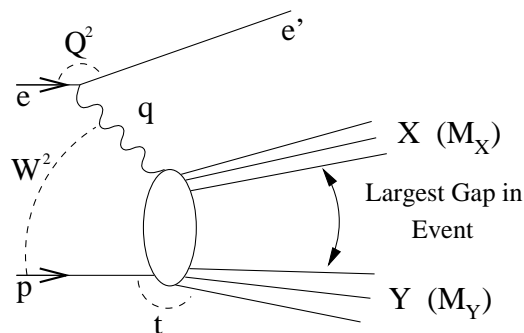


Figure 11:
Schematic representation of a DIS event with a rapidity gap.

3.1 Inclusive DIS diffraction

One of the surprises which came along with the first results from HERA was the observation of DIS events with a large rapidity gap in the hadronic final state, located between the photon and the proton fragmentation regions^{6,7} as depicted in figure 11. In the fragmentation picture driven by parton radiation large rapidity gaps are exponentially suppressed.⁵⁵ The observed fraction of events with large rapidity gaps is of the order of 10% fairly independent of W and Q^2 . This property is typical of diffractive scattering and invokes the notion of the Pomeron. The fact that the diffractive exchange can be probed with high Q^2 virtual photons means that its structure can be studied much the same way as the partonic structure of the proton.

Diffractive events in DIS at low x were expected^{56,57,58,59} long before they were observed. There are various ways of understanding it. The most compelling way is to think of the $\gamma^* p$ interaction in the rest frame of the proton. In this frame the life time of a $q\bar{q}$ fluctuation of the virtual photon can be estimated to be⁶⁰

$$\tau_{q\bar{q}} \simeq \frac{1}{2m_p x}, \quad (14)$$

where m_p denotes the mass of the target proton. At $x = 10^{-4}$, $c\tau_{q\bar{q}} \simeq 10^3$ fm is much larger than the typical size of a hadronic target. The photon may thus fluctuate into a $q\bar{q}$ pair long before arrival on target. The preferred configuration is the one in which the quarks have a relatively small transverse momentum, form a large size ob-

H1 Preliminary 1994

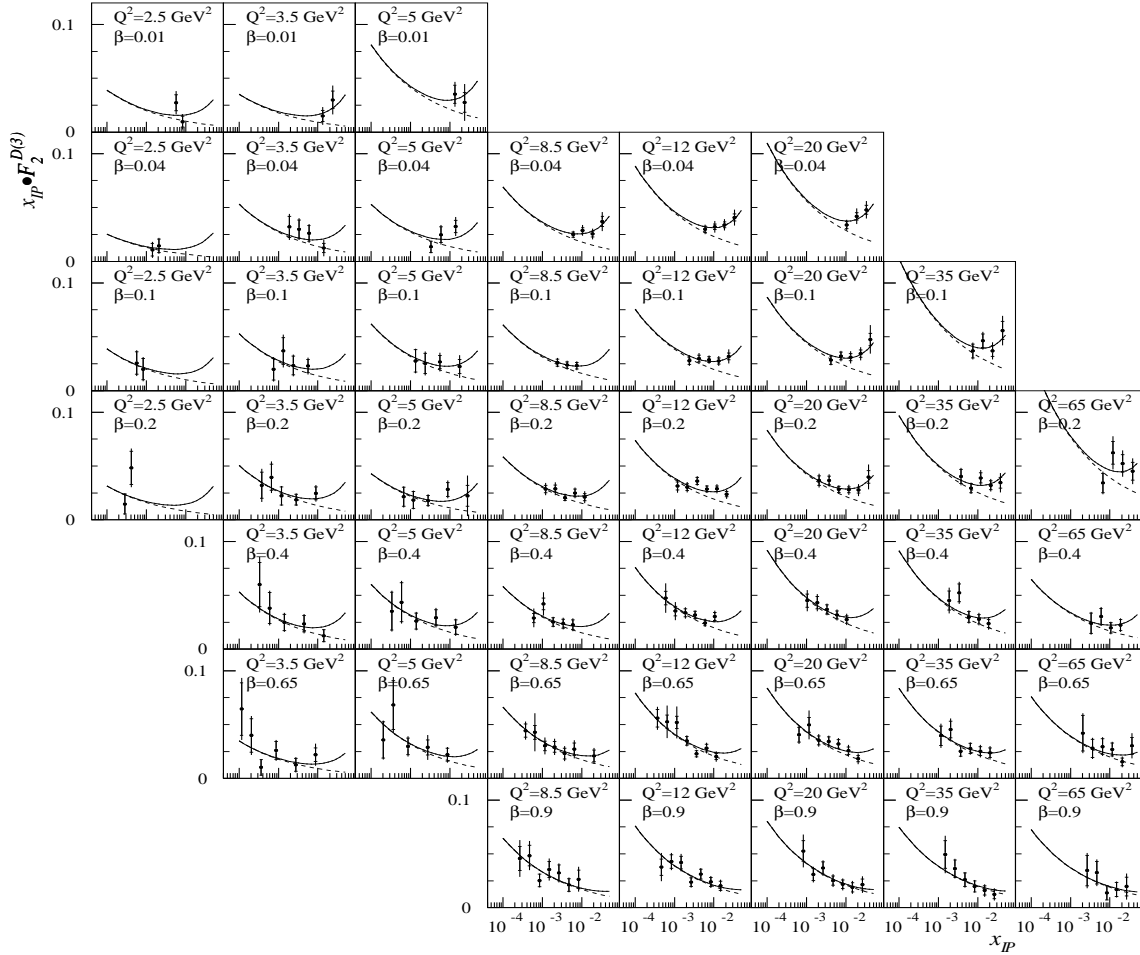


Figure 12: $x_P F_2^{D(3)}$ as a function of x_P in bins of β and Q^2 as denoted on the figure. The full line is the result of the fit of an incoherent sum of the P and f meson trajectories. The dashed line corresponds to the P contribution.

ject and the virtual photon turns into a hadronic probe. It is thus to be expected that the γ^*p interactions will be similar to hadron-hadron interactions. Of course QCD introduces corrections to the above picture, such as scaling violation or production of large p_T jets, all of which can be accommodated in the laboratory frame description.^{61,62} In this picture diffractive scattering emerges naturally, as a consequence of the hadronic-like nature of the virtual photon.

Assuming the validity of Regge factorization for γ^*p diffractive interactions (while ignoring the sub-leading Regge trajectories) we expect,

$$\frac{d^2\sigma(\gamma^*p)}{dtdx_P} = F_{P/p}(t, x_P)\sigma(\gamma^*P), \quad (15)$$

where $F_{P/p}(t, x_P)$ denotes the flux of the Pomeron in the proton, x_P is the fraction of the proton momentum carried by the Pomeron and t is the square of the four-momentum transfer at the proton vertex. We may define the DIS differential cross section (and the appropriate structure function) for producing a diffractive hadronic state X of mass M_X in the reaction $ep \rightarrow epX$,

$$\frac{d^3\sigma^D}{dx_P d\beta dQ^2} = \frac{2\pi\alpha^2}{\beta Q^4} [1 + (1-y)^2] F_2^{D(3)}(\beta, Q^2, x_P), \quad (16)$$

where β is defined as

$$\beta = \frac{x}{x_P} \simeq \frac{Q^2}{M_X^2 + Q^2}, \quad (17)$$

and an implicit integration over t is assumed in accordance with the experimental conditions. Should the Regge type factorization hold in the DIS regime, one expects

$$F_2^{D(3)}(\beta, Q^2, x_{\mathbb{P}}) = \frac{1}{x_{\mathbb{P}}^n} F_2^{\mathbb{P}}(\beta, Q^2), \quad (18)$$

with the structure function of the Pomeron, $F_2^{\mathbb{P}}$, defined by this equation. The first term stands for the flux of the Pomeron with $n = 1 - 2\alpha_{\mathbb{P}}(0) + \delta_t$, independent of β and Q^2 ($\delta_t \simeq 0.03$ is a correction due to the effect of α' in the integration over t). Experimentally $F_2^{D(3)}$ can be defined either at the hadronic level, by the presence of a large rapidity gap between X and the final state of the proton Y (see figure 11) which for most analyzes remains undetected or by tagging a fast proton in the forward spectrometer.

Tests of factorization have been conducted by the H1 Collaboration⁶³ in the range $2.5 < Q^2 < 65 \text{ GeV}^2$, $0.01 < \beta < 0.9$ and $10^{-4} < x_{\mathbb{P}} < 5 \cdot 10^{-2}$. As can be seen in figure 12 a change of the $x_{\mathbb{P}} F_2^{D(3)}$ dependence on $x_{\mathbb{P}}$ as a function of β is observed. However if a fit to $F_2^{D(3)}$ is performed assuming a contribution of both the Pomeron and the f meson trajectories the results are consistent with the intercepts of the two trajectories being independent of β and Q^2 as expected for Regge factorization. The intercept of the f trajectory is compatible with the expectations ($\alpha_f \simeq 0.6$) while that of the Pomeron,

$$\alpha_{\mathbb{P}}(0) = 1.18 \pm 0.02(\text{stat}) \pm 0.07(\text{syst}),$$

is within errors marginally higher than would be expected for a soft Pomeron.^a A similar intercept,

$$\alpha_{\mathbb{P}}(0) = 1.17 \pm 0.04(\text{stat}) \pm 0.08(\text{syst}),$$

has been obtained by the ZEUS Collaboration in a measurement performed with the Leading Proton Spectrometer⁶⁵ (LPS) at an average $Q^2 =$

^aThe value of $\alpha_{\mathbb{P}}$ measured in the energy dependence of the DIS diffractive cross section by the ZEUS Collaboration^{64,65} has been found substantially larger than the value from soft interactions. However recently a technical mistake has been found in the generation of the Monte Carlo data used for the acceptance correction and resolution unfolding. This mistake led to the mishandling of QED radiative corrections. Its effect is to change the cross sections by typically one systematic error. The ZEUS collaboration thus has retracted their results until further analysis is completed.

12 GeV^2 for the range $0.006 < \beta < 0.5$ and $4 \cdot 10^{-4} < x_{\mathbb{P}} < 3 \cdot 10^{-2}$. In this measurement the scattered proton, with a fraction of the initial proton momentum larger than 0.93, is detected in the LPS. The advantage of detectors such as the LPS is that the t distribution of the diffractive events can be studied. The $|t|$ distribution measured in the range $0.07 < |t| < 0.35 \text{ GeV}^2$, corrected for detector acceptance and resolution, is presented in figure 13. Assuming an exponential fall-off in $|t|$, the fitted slope is determined to be $b = 5.9 \pm 1.3_{-0.7}^{+1.1} \text{ GeV}^{-2}$. This value is within errors compatible with expectations based on the soft Pomeron phenomenology.

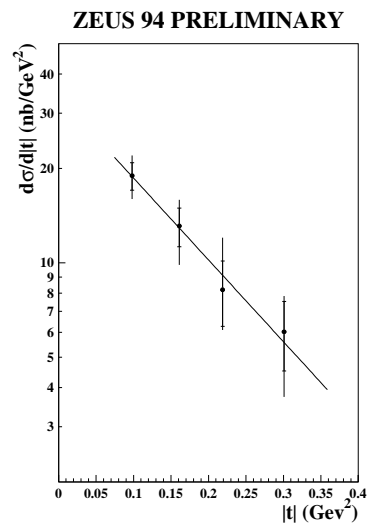


Figure 13:
The t distribution of diffractive DIS as measured with the LPS.

The Q^2 dependence in bins of β of $\tilde{F}_2^D = \int F_2^{D(3)} dx_{\mathbb{P}}$, where the integration is over $3 \cdot 10^{-4} < x_{\mathbb{P}} < 5 \cdot 10^{-2}$, as determined by the H1 experiment is presented in figure 14. While the β dependence is very weak, the striking observation is that at large β there is almost no Q^2 dependence. A slight rise with Q^2 is evident at low β . The structure function F_2^D is directly proportional to $F_2^{\mathbb{P}}$. If Regge factorization holds, one would expect the Q^2 dependence of $F_2^{\mathbb{P}}$ to be governed by the DGLAP evolution equations. In this case the lack of Q^2 dependence at large β can only be explained by a large gluon contribution at large β which would compensate the expected deple-

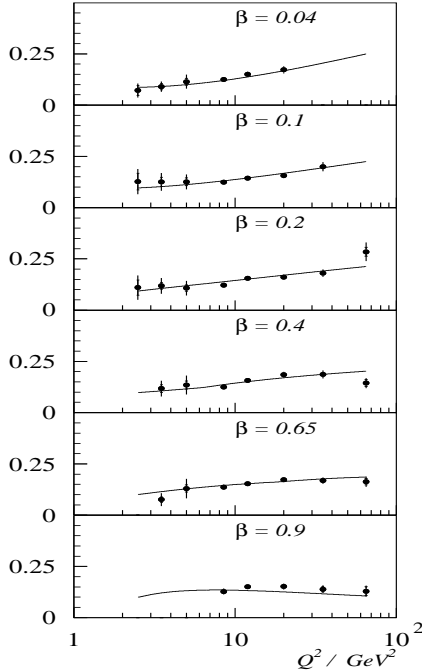


Figure 14:

The Q^2 dependence of $\tilde{F}_2^D \sim F_2^P$ in bins of β . The lines are the result of a QCD fit with quarks and gluons present at the starting scale of $Q_0^2 = 2.5 \text{ GeV}^2$.

tion of fast quarks due to radiation. Indeed the initial conditions needed to fulfill the NLO QCD evolution of F_2^P , as obtained from a fit performed by H1, favor a gluon distribution strongly peaked at fraction of \mathbb{P} momentum close to unity and a flat quark distribution. As seen in figure 15 more than 80% of the Pomeron momentum is carried by (hard) gluons, at least in the Q^2 range available in this study.

3.2 DIS vector meson production

Another diffractive reaction which was investigated at HERA is the exclusive vector meson (VM) production in DIS, $ep \rightarrow epV$. The interest in measuring this process was generated by the calculations of VM production in two-gluon exchange models.^{66,67,68} Two-gluon exchange is a prototype for modeling the Pomeron exchange.^{69,70} It turns out that for a longitudinally polarized photon perturbative QCD calculations can be applied strictly and the applicability of the QCD factorization theorem implies that the scattering amplitude

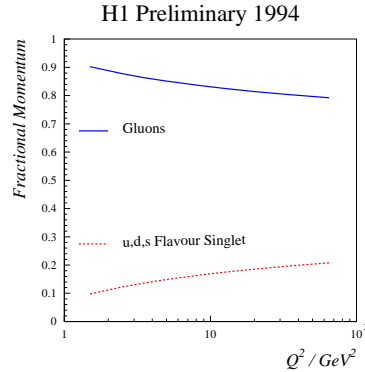


Figure 15:

The fraction of the \mathbb{P} momentum carried by gluons and light quarks as a function of Q^2 as determined from a QCD fit.

is proportional to the gluon distribution in the proton.^{68,71} The contribution of the longitudinal polarization is expected to dominate at large Q^2 , independently of other model assumptions. Thus in all the models, at small x

$$\frac{d\sigma}{dt} \propto \frac{\alpha_s^2(Q^2)}{Q^6} |xg(x, Q^2)|^2, \quad (19)$$

however the nature of the exchanged gluons in the VM production mechanism is subject to heated debates (for a review see⁷²).

Should the QCD expectations be fulfilled in the data, hard diffractive VM production may turn out to be the way to measure the gluon distribution in the proton, to study the approach to the unitarity limit and even to investigate the properties of the VM wave functions. There are indications that the perturbative production mechanism is present. The measurements of the Q^{-2a} dependence of the ρ^0 and J/ψ production cross sections favor a value of $a \simeq 2$ with an error typically of 20%.^{73,74} In photoproduction the SU(4) flavor symmetry is badly broken. In QCD one expects the SU(4) symmetry to be restored at large Q^2 . This seems to be borne out by the data as can be seen in figure 16 where the measured rates of various VM production relative to the ρ^0 are shown at $Q^2 = 0 \text{ GeV}^2$ and for higher Q^2 .^{73,74,75,76} The most spectacular is the increase of the J/ψ to ρ^0 production ratio which approaches unity at $Q^2 = 20 \text{ GeV}^2$.

Should the gluons mediating the VM production be perturbative in nature, one expects the

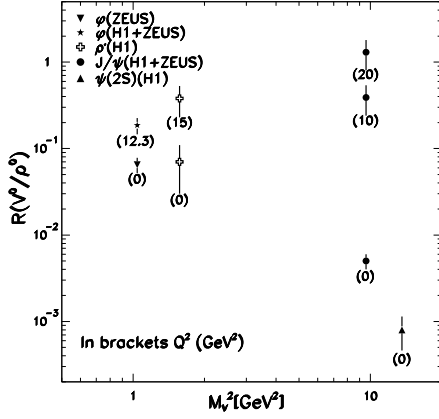


Figure 16:

Production rate of vector mesons relative to ρ^0 as a function of their mass square M_V^2 for different values of Q^2 .

cross section to increase with W as the square of the gluon distribution, that is, much faster than for the soft Pomeron. At high Q^2 the HERA measurements are not precise enough to determine the W dependence consistently within one experiment. Relative to the NMC measurements⁷⁷ the rise of the cross section is much stronger than expected for non-perturbative production mechanisms. Also the W dependence of the J/ψ photoproduction cross section is stronger than for the soft Pomeron^{78,79} and in accord with the perturbative approach.^{67,80} A compilation of the existing measurements of ρ^0 is presented in figure 17.

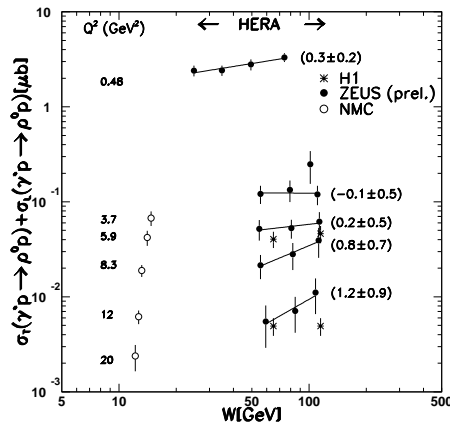


Figure 17:

The ρ^0 cross section as a function of W for different γ^* virtualities Q^2 . The numbers in parenthesis are the values of the power a of a fit W^a to the ZEUS data.

The contribution of the longitudinal photon relative to the transverse photon, R , can be determined from the polarization of the vector meson and assuming s-channel helicity conservation. As expected R is increasing with Q^2 , as shown in figure 18, and this increase is well reproduced by perturbative calculations which assume hadron-parton duality.⁸¹ The decrease of the size of the

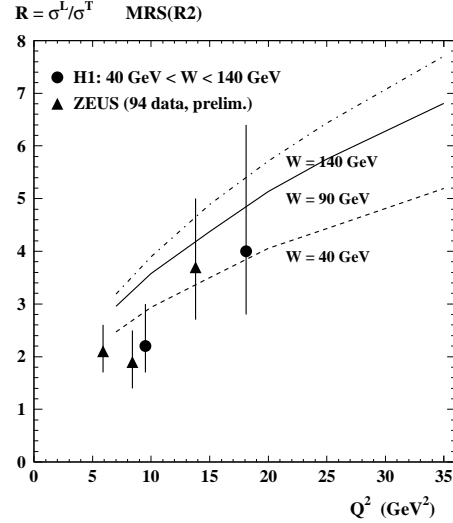


Figure 18:

The ratio R of longitudinal to transverse ρ^0 polarization as a function of Q^2 compared to perturbative model calculations.⁸¹

interacting photon is also observed in the behavior of the slope b of the t distribution. This can be seen in figure 19 where b measured for exclusive ρ^0 production is plotted as a function of Q^2 . The b dependence as a function of W in DIS is compatible with $\alpha' = 0.25 \text{ GeV}^{-2}$ as in the case of reactions mediated by the soft Pomeron (see figure 20).

3.3 Conclusions

The intercept of the Pomeron as measured in DIS seems higher than the one of the Pomeron mediating soft interactions. At this point it is not clear whether we are probing the same object and it might be wiser to use the notion of an effective Pomeron. Assuming the validity of the DGLAP evolution for inclusive diffractive scattering, it is found that the effective Pomeron consists mainly of hard gluons. There are some indications that it develops differently in exclusive processes when

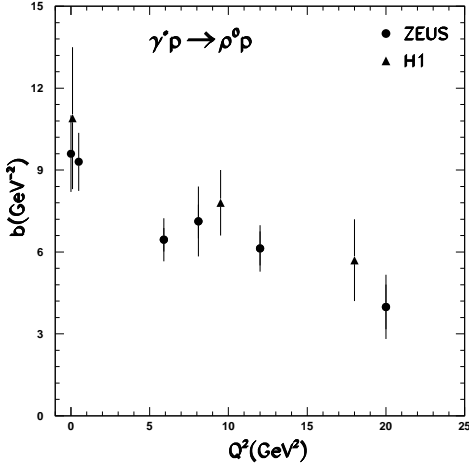


Figure 19:

The slope b of the exponential t dependence $\exp(-b|t|)$ for ρ^0 production as a function of the photon virtuality Q^2 .

$M_X^2 \ll Q^2$. We may be witnessing the fact that the Pomeron is not a universal object. However, before this conclusion can be reached on solid grounds more precise measurements are needed.

4 The photon structure function

The photon is probably the most interesting particle to study. It is one of the gauge particles of the Standard Model and as such has no intrinsic structure. However it acquires a structure in its interactions with matter and in that sense it is a prototype for studying the formation of a partonic object.

The structure functions of the photon are defined in DIS $e\gamma \rightarrow eX$ through the interaction cross section,

$$\frac{d^2\sigma}{dx dQ^2} = \frac{2\pi\alpha^2}{xQ^4} [(1 + (1 - y)^2) F_2^\gamma - y^2 F_L^\gamma] . \quad (20)$$

In the quark-parton model the contribution to this cross section comes from the so called box diagram $\gamma^*\gamma \rightarrow q\bar{q}$. Should this be the only contribution, the structure function of the photon could be fully calculated in QCD. In reality the real photon can fluctuate into partonic states and in particular into a vector meson state. Thus the overall contribution to the cross section is more complicated. This has also implications for the evolution equation of

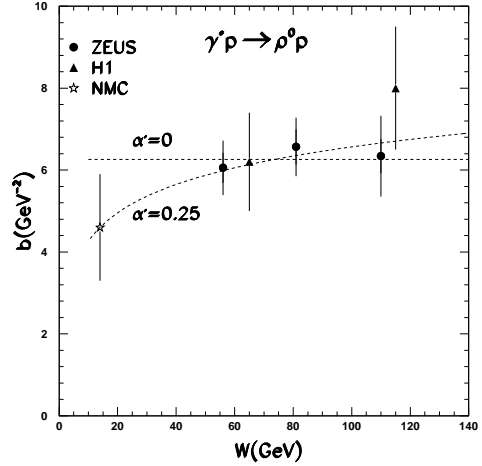


Figure 20:

The slope b of the exponential t dependence $\exp(-b|t|)$ for ρ^0 production at $Q^2 \simeq 10 \text{ GeV}^2$ as a function of W .

the photon structure function. In particular the box contribution mentioned above introduces an extra splitting function into the evolution equation, that of a photon splitting into a $q\bar{q}$. The latter is responsible for the fact that $F_2^\gamma(x, Q^2)$ is large at large x and increases with Q^2 at any value of x .

Experimentally F_2^γ is measured in e^+e^- interactions, by requiring that one of the electrons scatters under small angles and remains undetected (the source of the target photon) while the second one scatters under a large angle, providing the probing virtual photon. New data have been presented^{82,83} on the measurements of the $\gamma^*\gamma$ interactions from the LEP experiments. The OPAL experiment⁸² has presented results on F_2^γ with improved resolution, thanks to the use of their forward detectors.

The x dependence of F_2^γ in bins of Q^2 is shown in figure 21. For the sake of comparison with the proton structure function the scale of x was chosen logarithmic. The measurements are compared to three different sets of parton distributions in the photon.^{84,85,86} At higher x , where data are available, all the parameterizations describe F_2^γ well. The largest differences are seen at low x . This is not unlike the parameterizations of the proton structure function which were available before the low x measurements at HERA. In the case of the photon, the situation is thought to be worse since

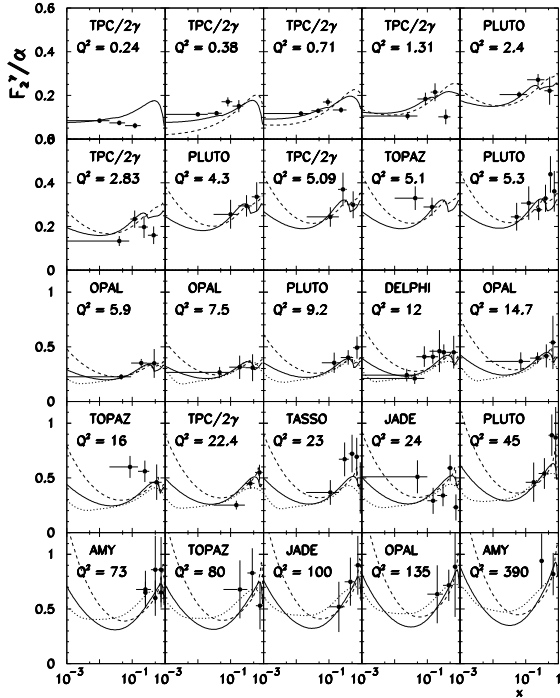


Figure 21:

The photon structure function F_2^γ/α as a function of x in bins of Q^2 compared to the LO GRV⁸⁴ (dashed line), GS⁸⁵ (dotted line) and SaS⁸⁶ (full line) parameterizations of parton distributions in the photon.

no momentum sum rule is used to constrain the gluon distribution. However recently such a sum rule has been derived.⁸⁷

The uncertainty in the gluon distribution can be partly minimized by the hard photoproduction data from the HERA experiments⁸⁸ $\gamma p \rightarrow jet_1 + jet_2 + X$. An example of the potential of HERA is shown in figure 22, where an effective structure function of the photon is plotted as a function of the transverse momentum square of the jets, for various ranges of x of the photon.

5 Summary

The F_2 structure function of the proton has been measured with high precision in the range $10^{-6} < x < 1$ and $0.1 < Q^2 < 5000 \text{ GeV}^2$. The DGLAP evolution equation in NLO describes the data very consistently and down to $Q^2 \simeq 1 \text{ GeV}^2$. However

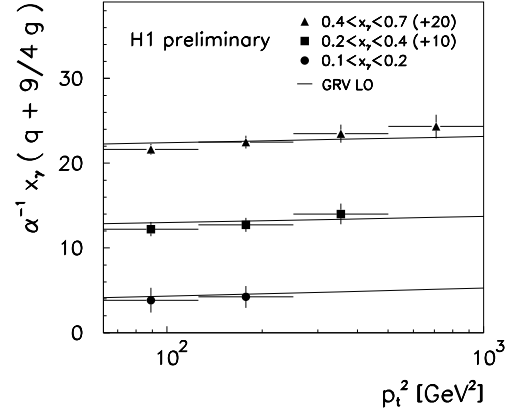


Figure 22:

Effective structure function of the photon as measured in photoproduction of two jets with high transverse momentum p_t .

the contribution of non-conventional QCD dynamics cannot be ruled out without further studies.

Hard diffractive scattering, first sign of coherent phenomena in perturbative QCD, allows to probe directly the nature of strong interactions. It can further help to constrain the gluon distribution in the proton.

With the LEP and HERA experiments measuring the partonic structure of the photon we are slowly approaching the low x regime in photon induced reactions.

Given the large theoretical support and interest in the low x phenomena, we should soon be able to achieve a good understanding of QCD dynamics of high parton densities. One of the outcomes will be reliable parton distributions for the next generation colliders.

Acknowledgments

It is a pleasure for me to thank all my colleagues from the different experiments for useful discussions. Very special thanks go to E. Gurvich, A. Levy and E. Rondio for preparing some of the compilation figures. I am grateful for the help of R. Klanner, A. D. Martin and R. G. Roberts in preparing this talk. I would like to acknowledge many enlightening discussions with J. Bartels, W.

Buchmüller and L. Frankfurt. Last but not least I would like to thank the organizers and colleagues from Warsaw University (my Alma Mater) for their warm hospitality.

This work was partially supported by the German Israeli Foundation, the Minerva Foundation and DESY.

References

1. A. Donnachie, P. V. Landshoff, *Nucl. Phys.* **B 231** (1983) 189.
2. A. Donnachie, P. V. Landshoff, *Nucl. Phys.* **B 244** (1984) 322.
3. A. Donnachie, P. V. Landshoff, *Nucl. Phys.* **B 267** (1986) 690.
4. A. Donnachie, P. V. Landshoff, *Phys. Lett.* **B 296** (1992) 227.
5. A. Donnachie, P. V. Landshoff, *Phys. Lett.* **B 202** (1988) 131.
6. ZEUS Collaboration; M. Derrick et al., *Phys. Lett.* **B 315** (1993) 481.
7. H1 Collaboration; T. Ahmed et al., *Nucl. Phys.* **B 429** (1994) 477.
8. NMC Collaboration; M. Arneodo et al., *hep-ph/9610231* (1996).
9. H1 Collaboration; S. Aid et al., *Nucl. Phys.* **B 470** (1996) 3.
10. ZEUS Collaboration; M. Derrick et al., *Z. Phys.* **C 69** (1996) 607.
11. L. W. Whitlow et al., *Phys. Lett.* **B 282** (1992) 475.
12. BCDMS Collaboration; A. C. Benvenuti et al., *Phys. Lett.* **B 233** (1989) 485.
13. BCDMS Collaboration; A. C. Benvenuti et al., *Phys. Lett.* **B 237** (1990) 592.
14. E665 Collaboration; M. R. Adams et al., *Phys. Rev.* **D 54** (1996) 3006.
15. W. J. Stirling, in *International Workshop on Deep Inelastic Scattering and Related Phenomena*, edited by G. D'Agostini, A. Nigro (Rome, 1996), hep-ph/9608411.
16. G. Sterman, in *28th International Conference on High Energy Physics* (Warsaw, 1996), these proceedings and hep-ph/9610462.
17. A. D. Martin, W. J. Stirling, R. G. Roberts, *Phys. Rev.* **D 50** (1994) 6734.
18. M. Glück, E. Reya, A. Vogt, *Z. Phys.* **C 67** (1995) 433.
19. CTEQ Collaboration; R. Brock et al., *Rev. Mod. Phys.* **67** (1995) 157.
20. ZEUS Collaboration; M. Derrick et al., *Z. Phys.* **C 63** (1994) 391.
21. H1 Collaboration; S. Aid et al., *Z. Phys.* **C 69** (1995) 27.
22. ZEUS Collaboration; J. Parsons for the Collaboration, pa02-047, submitted to this conference.
23. H1 Collaboration; V. Skeleyan for the Collaboration, pa02-060, pa02-069, pa02-70, submitted to this conference.
24. A. Donnachie, P. V. Landshoff, *Z. Phys.* **C 61** (1994) 139.
25. A. Capella et al., *Phys. Lett.* **B 337** (1994) 358.
26. B. Badełek and J. Kwieciński, *Phys. Lett.* **B 295** (1992) 263.
27. V. N. Gribov, L. N. Lipatov, *Sov. J. Nucl. Phys.* **15** (1972) 438,675.
28. Y. L. Dokshitzer, *Sov. Phys. JETP* **46** (1977) 641.
29. G. Altarelli, G. Parisi, *Nucl. Phys.* **B 126** (1977) 298.
30. V. Fadin, E. Kuraev, L. Lipatov, *Sov. Phys. JETP* **44** (1976) 443.
31. V. Fadin, E. Kuraev, L. Lipatov, *Sov. Phys. JETP* **45** (1977) 199.
32. Y. Balitski, L. Lipatov, *Sov. J. Nucl. Phys.* **28** (1978) 822.
33. M. Ciafaloni, *Nucl. Phys.* **B 296** (1988) 49.
34. G. Marchesini, *Nucl. Phys.* **B 445** (1995) 49.
35. S. Catani, F. Fiorani, G. Marchesini, *Nucl. Phys.* **B 336** (1990) 18.
36. A. D. Martin, in *International Workshop on Deep Inelastic Scattering and Related Phenomena*, edited by G. D'Agostini, A. Nigro (Rome, 1996), (see for discussion).
37. A. D. Martin, R. G. Roberts, W. Stirling, *Phys. Lett.* **B 354** (1995) 155.
38. A. D. Martin, R. G. Roberts, W. J. Stirling, *RAL-TR-96-037* (1996).
39. M. Glück, E. Reya, A. Vogt, *Z. Phys.* **C 53** (1992) 127.
40. H. L. Lai et al., *Phys. Rev.* **D 51** (1995) 4763.
41. S. Catani, *hep-ph/9609263* (1996).
42. S. Catani, *hep-ph/9608310* (1996).
43. R. G. Roberts, *J. Phys.* **G 22** (1996) 675.
44. L. W. Whitlow et al., *Phys. Lett.* **B 250**

- (1990) 193.
45. CCFR Collaboration; D. Harris for the Collaboration, pa03-030, submitted to this conference.
 46. CCFR Collaboration; A. Bodek et al, *hep-ex/9605005* (1996).
 47. B. Badełek, J. Kwieciński, A. Staśto, *hep-ph/9603230* (1996).
 48. E. M. Levin et al., *hep-ph/9606443* (1996).
 49. ZEUS Collaboration; M. Derrick et al., pa02-031, submitted to this conference.
 50. G. Ingelman, J. Rathsman, G. A. Schuler, *hep-ph/9605285* (1996).
 51. EMC Collaboration; J. J. Aubert et al., *Nucl. Phys. B* **213** (1983) 31.
 52. M. Virchaux, A. Milsztajn, *Phys. Lett. B* **274** (1992) 221.
 53. J. Busenitz, in *International Europhysics Conference on High Energy Physics*, edited by F. V. J. Lemonne, C. Vander Velde (Brussels, 1995).
 54. H1 Collaboration; E. Mroczko for the Collaboration, pa02-076, submitted to this conference.
 55. Y. L. Dokshitzer et al., *Basics of perturbative QCD* (Ed. Frontieres, 1991).
 56. J. Bjorken, in *Proceedings of the International Symposium on Electron and Photon Interactions at High Energies* (Cornell, 1971), p. 281.
 57. A. Donnachie, P. V. Landshoff, *Phys. Lett. B* **191** (1987) 309.
 58. G. Ingelman, P. Schlein, *Phys. Lett. B* **152** (1985) 256.
 59. N. Nikolaev, B. Zakharov, *Z. Phys. C* **53** (1992) 331.
 60. H. Abramowicz, L. Frankfurt, M. Strikman, *DESY-95-047* (1995).
 61. H. Abramowicz et al., in *Future Physics at HERA (Workshop)* (DESY, Hamburg, 1996).
 62. W. Buchmuller, M. F. McDermott, A. Hebecker, *hep-ph/9607290* (1996).
 63. H1 Collaboration; J. P. Phillips for the Collaboration, pa02-061, submitted to this conference.
 64. ZEUS Collaboration; M. Derrick et al., *Z. Phys. C* **70** (1996) 391.
 65. ZEUS Collaboration; G. Barbagli for the Collaboration, pa02-026, submitted to this conference.
 66. A. Donnachie, P. V. Landshoff, *Phys. Lett. B* **185** (1987) 403.
 67. M. G. Ryskin, *Z. Phys. C* **57** (1993) 89.
 68. S. Brodsky et al., *Phys. Rev. D* **50** (1994) 3134.
 69. F. E. Low, *Phys. Rev. D* **12** (1975) 163.
 70. S. Nussinov, *Phys. Rev. Lett.* **334** (1975) 1286.
 71. L. Frankfurt, W. Koepf, M. Strikman, *Phys. Rev. D* **54** (1996) 3194.
 72. W. Koepf et al., in *Future Physics at HERA (Workshop)* (DESY, Hamburg, 1996).
 73. H1 Collaboration; S. Aid et al., *Nucl. Phys. B* **468** (1996) 3.
 74. ZEUS Collaboration; J. Bulmahn for the Collaboration, pa02-028, submitted to this conference.
 75. H1 Collaboration; J. Gayler for the Collaboration, pa01-088, pa02-064, pa02-066, pa02-86, submitted to this conference.
 76. ZEUS Collaboration; M. Derrick et al., *Phys. Lett. B* **380** (1996) 220.
 77. NMC Collaboration; M. Arneodo et al., *Nucl. Phys. B* **429** (1994) 503.
 78. H1 Collaboration; S. Aid et al., *Nucl. Phys. B* **472** (1996) 3.
 79. ZEUS Collaboration; M. Derrick et al., *Phys. Lett. B* **350** (1995) 120.
 80. M. G. Ryskin et al., *hep-ph/9511228* (1995).
 81. A. D. Martin, M. G. Ryskin, T. Teubner, *hep-ph/9609448* (1996).
 82. OPAL Collaboration; J. Lauber for the Collaboration, pa03-007, submitted to this conference.
 83. DELPHI Collaboration; Y. Tyapkin for the Collaboration, pa02-021, submitted to this conference.
 84. M. Gluck, E. Reya, A. Vogt, *Phys. Rev. D* **45** (1992) 3986.
 85. L. E. Gordon, J. K. Storrow, *Z. Phys. C* **56** (1992) 307.
 86. G. A. Schuler, T. Sjostrand, *Z. Phys. C* **68** (1995) 607.
 87. L. L. Frankfurt, E. G. Gurvich, *hep-ph/9505406* (1995), pa03-033, submitted to this conference.
 88. H1 Collaboration; M. Erdmann for the Collaboration, pa02-080, submitted to this conference.